Materials Today Communications 27 (2021) 102252

Contents lists available at ScienceDirect

Materials Today Communications

journal homepage: www.elsevier.com/locate/mtcomm

Sensing capability and diameter-dependent electronic structure of boron nitride nanotubes

İskender Muz [a], Sholeh Alaei [b], Mustafa Kurban [c,*]

[a] Department of Mathematics and Science Education, Nevşehir Hacı Bektas Veli University, 50300, Nevşehir, Turkey
[b] Department of Physics, Urmia Branch, Islamic Azad University, Urmia, Iran
[c] Department of Electrical and Electronics Engineering, Kırşehir Ahi Evran University, 40100 Kırşehir, Turkey

ARTICLE INFO

Keywords:
Boron nitride nanotube
Diameter-dependence
CO adsorption
DFT

ABSTRACT

The sensing and diameter-dependent properties of armchair Boron Nitride nanotubes (BNNTs) were scrutinized based on density functional theory (DFT) to find out their electronic structure and carbon monoxide (CO) sensing capability. Our results show that diameter increase causes a rise in the binding energy of BNNT, from 6.44 eV to 6.62 eV. An increasing trend of adsorption energies in the range of -3.25 and -3.47 kcal/mol indicates that BNNTs act weak physical adsorption upon CO verified by the analysis of the Electron localization function (ELF), however, more increase in the diameter could enhance the sensing capability of BNNT. The energy gap of the biggest BNNT is calculated as 6.20 eV wide, i.e., about 0.12 eV smaller than the smallest one which is compatible with available experimental results. The reactivity properties such as the adiabatic and vertical ionization potentials (IPs), chemical hardness, and electrophilicity index of BNNTs were also analyzed. The BNNTs exhibit strong absorption peaks ~7.08 eV which can be a promising candidate for the UV light-emitting devices. The results herein reveal that BNNTs with bigger diameters can be useful for gas sensor applications.

1. Introduction

Carbon nanotubes (CNTs) have widely been used in the recent years due to their easy synthesis in a laboratory with high quality, however, some obstacles such as the non-ideal structure bringing about relatively high resistivity, the large number of thermal defects and chirality-dependent electronic characteristics, make them difficult to be applied in semiconductor devices. To make up for these difficulties, recently, inorganic nanotubes including B, N, Al, Si, Ga, and Ge atoms have been proposed in both experimental and theoretical studies. Among them, boron nitride nanotubes (BNNTs) have been a novel class of materials that have offered outstanding and have unique features for industrial, technical, electronic, and scientific applications in the past decades. BNNTs, as a type ofone-dimensional (1D) nanomaterials such as CNTs, have earned a strong reputation in various fields of electronic and optoelectronic devices [1–3] in view of their intriguing chemical, physical, and mechanical properties [4–6]. BNNTs are composed of B and N atoms with a bandgap of 6 eV which arises from the high electronegativity of a nitrogen atom. B and N atoms in a honeycomb lattice are covalently bonded to each other and are an insulator regardless of the helicity, nanotube wall numbers and diameters [7,8], while CNTs are semimetallic and semiconducting material. However, according to Zhang and co-workers [9], the energy gaps of small BNNTs with diameters below 4 Å are dependent on the chirality and diameters as indicated by quantum mechanical calculations. They found that the BNNTs have desirable orbital energies and demonstrate strange distribution of nearly free electron states owing to strong orbital hybridization effect. The conflict in electronic properties of BNNTs is related to the polarity in B—N bond resulting from the difference in electronegativity of B and N [10], thus the bonding electrons of BNNT are mainly accumulated around N atoms with an asymmetric charge distribution. Herein, the peculiar electronic structure ensures them to be a good candidate for applications in electronic, optical, and optoelectronic devices. However, the wide bandgap restricts the field of applications of BNNTs, therefore, from the technological point of view, it should be pointed out finding methods for tuning the bandgap of BNNTs and the claim of tailoring the electronic energy gap of these BNNTs is of great interest. Moreover, doping the BNNTs with dopants is a method to reduce its band gap, so that BNNTs can be used as quantum wires. Much research has been undertaken in this regard to research the influence of doping and impurities on the electronic properties of BNNTs. Zhao and coworkers [11] and Zhukovskii et al. [12] have studied carbon-doped

* Corresponding author.
E-mail address: mkurbanphys@gmail.com (M. Kurban).

https://doi.org/10.1016/j.mtcomm.2021.102252
Received 31 January 2021; Received in revised form 12 March 2021; Accepted 13 March 2021
Available online 16 March 2021

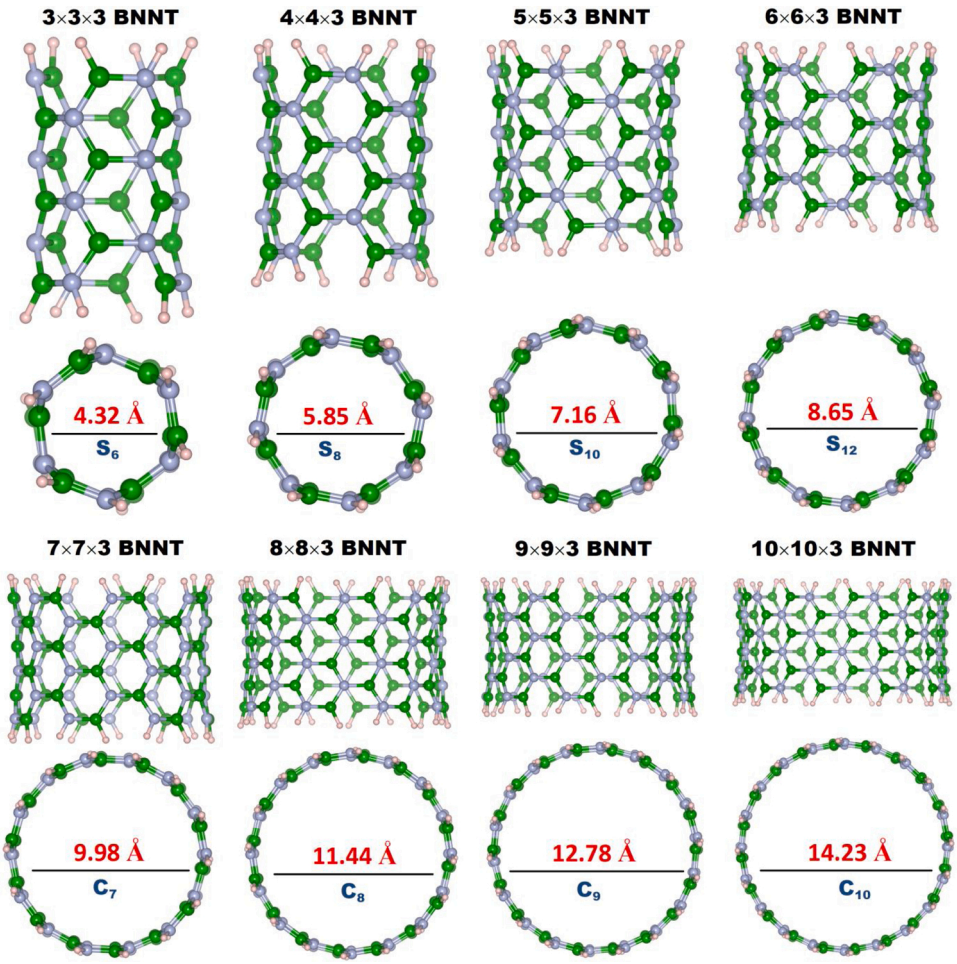

Fig. 1. Side and top views of optimized BNNT models with different diameters.

BNNTs and Oxygen dopant BNNTs, respectively. Bandgap reduction bringing about changes in the electronic properties of BNNTs are reported in some studies [13–15]. BNNTs as gas sensors, on the other hand, have been attracted in many studies. In this context, CO, NO_2, HCN, H_2, O_2, and HCHO upon BNNTs have been carried out to get insight into the sensing capability of BNNTs [16–28]. The main scope of these studies mentioned above is related to one BNNT model or Si, Ni, Pd, Pt, Ge-doped BNNTs. When it comes to CO upon BNNT interactions, zigzag (6,0) and armchair (3,3) [20], Ge-doped (8, 0) [21] and pristine (5,0) BNNTs [28] have been examined based on quantum mechanical calculations.

In this study, we conduct a comprehensive study, for the first time, to predict the diameter-dependent electronic structure of BNNTs and CO upon BNNTs with different diameters in detail. The studied stable BNNTs indicate their structural and electronic properties depending on diameter with the same chirality and exhibit unique electronic structure like their large-insulated family members. The binding energy, the Highest Occupied Molecular Orbital (HOMO), Lowest Unoccupied Molecular Orbital (LUMO), HOMO-LUMO energy gap, density of states (DOS), adiabatic ionization potential and vertical ionization potential, chemical hardness, electrophilicity index are reported. Using time-dependent density functional theory (TD-DFT) calculations, absorbance spectra of BNNTs with different diameters as a function of wavelength are also studied and predicted values compared with available experimental and theoretical results.

2. Computational details

In this study, we focus on armchair BNNTs including $3 \times 3 \times 3$, $4 \times 4 \times 3$, $5 \times 5 \times 3$, $6 \times 6 \times 3$, $7 \times 7 \times 3$, $8 \times 8 \times 3$, $9 \times 9 \times 3$ and $10 \times 10 \times 3$ type BNNT, in whose cell there are 48 ($B_{18}N_{18}H_{12}$), 64 ($B_{24}N_{24}H_{16}$), 80 ($B_{30}N_{30}H_{20}$), 96 ($B_{36}N_{36}H_{24}$), 112 ($B_{42}N_{42}H_{28}$), 128 ($B_{48}N_{48}H_{32}$), 144 ($B_{54}N_{54}H_{36}$) and 160 ($B_{60}N_{60}H_{40}$) atoms or BNNTs with various diameters, respectively. Both ends of the BNNTs were capped with hydrogen atoms to saturate dangling bonds due to fragment stabilization effect in the system [29]. All of the BNNTs have been optimized at the B3LYP/6-311G(d,p) level [30] by Gaussian09 [31] program based on the addition of an empirical dispersion term of Grimme's three-parameter [32] and Density Functional Theory (DFT). The same level of theory was also used for the vibrational frequency analysis.

The binding energy per atom (E_b) are calculated as following: $E_b = [i \times (E(B) + E(N)) + j \times E(H) - E(BNNT)]/(2i + j)$. The adiabatic ionization potential (AIP) and vertical ionization potential (VIP) were calculated using the following expression: $[AIP/VIP = E^{cation} - E^{neutral}]$. AIP is the energy difference between cationic and neutral clusters at their respective equilibrium geometries. VIP is the energy difference between the ground state of neutral and cationic clusters, optimized by the geometry of the neutral clusters. DOS plots were obtained by utilizing GaussSum program [33] in order to evaluate the changes in the HOMO and LUMO levels of BNNT s. Moreover, using Koopman theorem [34] by $I \approx -E_{HOMO}$ and $A \approx -E_{LUMO}$, chemical hardness (η), electrophilicity index (ω) and maximum amount of electronic charge index (ΔN_{tot}) were derived for all BNNTs from the following expressions: $\eta =$

Table 1
Structural, stability and binding properties of BNNTs. (Symm is point group symmetry, E_T (Hartree) is total energy, f (cm^{-1}) is the lowest vibrational frequency of BNNTs, E_b (eV) is binding energy, and E_{ads} (kcal/mol) is adsorption energy between BNNTs and CO molecule).

Models	Symm	E_T	f	E_b	E_{ads}
3 × 3×3	S_6	−1442.2075	110.889	6.44	28.78
4 × 4×3	S_8	−1923.1404	66.746	6.52	−3.25
5 × 5×3	S_{10}	−2404.0412	45.919	6.56	−3.26
6 × 6×3	S_{12}	−2884.9260	32.799	6.58	−3.14
7 × 7×3	C_7	−3365.8014	24.627	6.60	−3.39
8 × 8×3	C_8	−3846.6706	19.251	6.61	−3.21
9 × 9×3	C_9	−4327.5354	15.110	6.61	−3.44
10 × 10 × 3	C_{10}	−4808.3970	12.046	6.62	−3.47

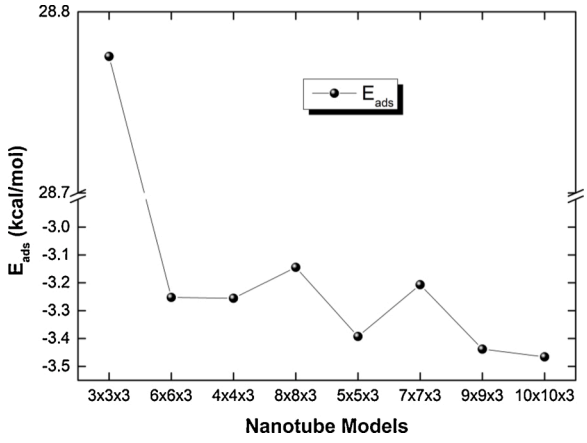

Fig. 2. The adsorption energy (E_{ads}) between BNNTs and CO.

(I-A)/2, $\omega = \mu^2/2\eta$ and $\Delta N_{tot} = -\mu/\eta$.

The adsorption energy (E_{ads}) of the CO upon the surface of BNNTs can be calculated as follows:

$$E_{ads} = E\left(\frac{BNNTs}{CO}\right) - E(BNNTs) - E(CO)$$

In addition, TD-DFT calculations have been carried out to evaluate ultraviolet-visible (UV-Vis) absorption spectra. For this part, we have used the CAM-B3LYP [35] functional because B3LYP functional underestimates exited state energies [36].

3. Results and discussion

The optimized structures of the armchair BNNTs including 3 × 3×3, 4 × 4×3, 5 × 5×3, 6 × 6×3, 7 × 7×3, 8 × 8×3, 9 × 9×3 and 10 × 10 × 3 BNNTs with various diameters from the side and top views are presented in Fig. 1. Structural parameters consisting of point group symmetry, energy, the lowest frequency, and the predicted value of energy gaps are listed in Table 1. As can be seen, the total energy (in Hartree) decreases with further increasing BNNT diameter. Frequency calculations were carried out for all structures and lower frequencies were obtained which affirms that all of them were minimum energy structures.

There are many physical properties based on symmetry such as selection rules, conducting properties, quantum numbers, etc. Furthermore, the symmetry of the BNNTs is useful for simplifying calculations. In this perspective, our results show that armchair BNNTs belong to different rod-group families, in agreement with [37] the point group symmetries of all BNNTs are calculated in Table 1 and it is seen that for 3 × 3×3, 4 × 4×3, 5 × 5×3, 6 × 6×3 BNNTs the point symmetries are S_6, S_8, S_{10} and S_{12}, respectively. For other BNNTs, 7 × 7×3, 8 × 8×3, 9 × 9×3 and 10 × 10 × 3, point groups are C_7, C_8, C_9 and C_{10}.

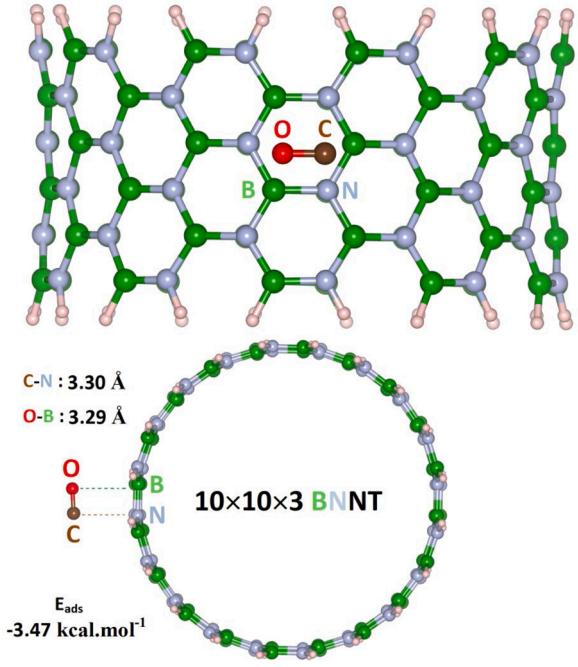

Fig. 3. The optimized geometry of side (up) and top (down) views and adsorption energy (E_{ads}) between 10 × 10 × 3 BNNT and CO molecule.

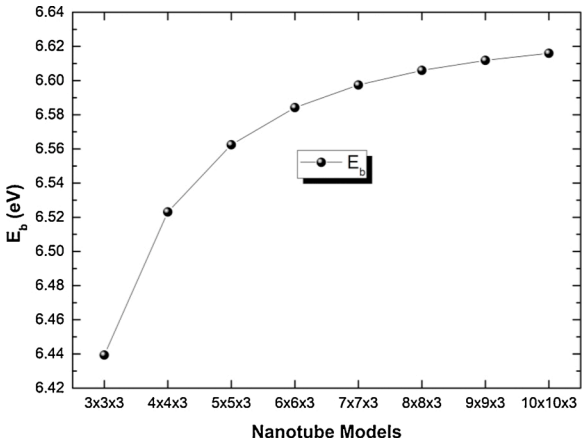

Fig. 4. The binding energy per atom (E_b) of BNNTs.

Fig. 2 reports the calculated binding energy per atoms (E_b) values as a function of the BNNTs. The E_b rises regularly as the diameter of BNNT increases. This also indicates that the stability increases with an increase in the BNNTs diameter. This trend is compatible with the E_b of carbon and aluminum nitride nanotubes [38,39]. In addition, the results showed that armchair BNNTs with even index n are centrosymmetric materials.

Fig. 3 shows the binding energies for the adsorption of CO on the surface of BNNTs. The adsorption energy of CO on the surface of 3 × 3×3 BNNT was calculated to be 28.78 kcal/mol, indicating an unfavorable adsorption process (see Table 1). However, the adsorption energy for 4 × 4×3 BNNT drops sharply with increasing diameter. Moreover, the adsorption behavior of CO on various diameters of BNNTs showed a similar trend: the adsorption energies were found to be in the range of -3.14 and -3.47 kcal/mol for CO adsorption on BNNT. This result means that, after CO, the BNNT/CO complexes are more stable with the negative adsorption energies. Comparing to the obtained trend of adsorption energies, 10 × 10 × 3 (-3.47) > 9 × 9×3 (-3.44) > 7 × 7×3 (-3.39) > 5 × 5×3 (-3.26) > 4 × 4×3 (-3.25) > 8 × 8×3

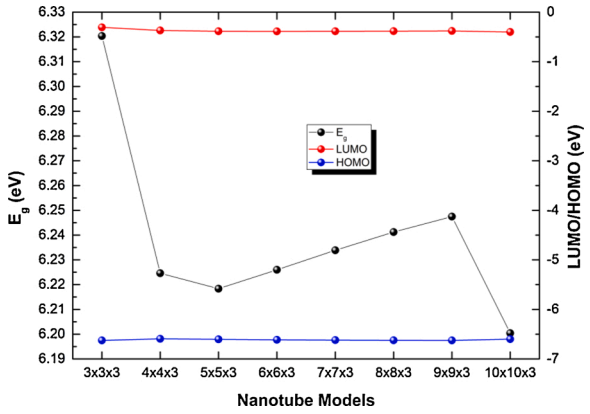

Fig. 5. The HOMO, LUMO and HOMO-LUMO energy gap (E_g) of BNNTs.

(-3.21) > 6 × 6×3 (-3.14) > 3 × 3×3 (28.78), it can be concluded that, the 10 × 10 × 3 BNNT are more favorable than others, as sensing device for CO (see Fig. 4). Overall, more increases in the diameter could enhance the sensing capability of BNNT over CO.

In Fig. 5, the HOMO and LUMO energy levels and corresponding energy gap versus BNNTs are plotted. This property is important for chemical stability and chemical reactivity. It is perceived that the energy gap is linked to the diameters of BNNTs. The parameters of these BNNTs show a decreasing trend with an increasing diameter of BNNT from 6.32 eV of 3 × 3×3 to 6.20 eV of 10 × 10 × 3. In other words, the energy gap shifts in the range of 6.32−6.20 eV going from the smallest to the largest diameter of BNNTs.

The energy gap can be correlated with the conductivity of the studied system. It is reported that the armchair BNNT have the energy gap between 5.0 and 6.2 eV independent of BNNT chirality [40,41] which provides good electrical insulation. However, CNTs can be metal or semiconductor. Table 2 presents the energy gap for various BNNTs. Calculated values for the energy gap are in good agreement with available theoretical and experimental results [42,43]. Introducing various diameters of BNNTs does not change the energy gap significantly suggesting that the electronic properties of the BNNTs remain the same upon further increase of diameters. The studies predicted that BNNTs with diameters smaller than 2 Å can exhibit semiconducting property with the energy gap around 1 eV, while for larger BNNTs, the energy gaps will be large. The predicted conclusions demonstrate that the electronic structure of various BNNTs depends on the diameter of BNNTs, which supplies useful guidance for the possible device applications of BNNT. Moreover, the change of the level of HOMO and LUMO orbitals affects the energy gap directly and thus other physiochemical properties such as chemical hardness or electrophilicity.

To better understand the band structure and electronic structure of the BNNTs, the density of states (DOS) of the BNNTs were also examined. Fig. 6 displays the DOS of 3 × 3×3, 4 × 4×3, 5 × 5×3, 6 × 6×3, 7 × 7×3, 8 × 8×3, 9 × 9×3 and 10 × 10 × 3 type BNNTs. The distributions of the DOS of BTTNs with smaller diameters are slightly different near the Fermi level, such as, for the BNNTs with diameter of 4.32 Å (3 × 3×3) and 8.65 Å (6 × 6×3). However, the scenario is different for larger BNNTs, i.e., for larger BNNTs with larger diameters DOS distribution is not the same as smaller ones near Fermi level. The analysis of the DOS demonstrated that the changes in the diameter of BNNTs have a clear influence on the DOS distribution near the Fermi level of the BNNTs. The band gaps become narrower as the diameter increases. It is evident that the diameter augmentation decreases the energy gap of armchair BNNT. Besides, there is available state, which is no localization within the energy gap, as it is seen in Fig. 6, representing insulator attitude of BNNT linked to wide-gap considerations, as expected.

All studied BNNTs show a strong insulator characteristic. Herein, the predictions in this study can provide useful information for the application of BNNTs on chemical properties such as catalysis reactivity, stability, and adsorption [44,45] and physical properties like conductivity, semiconductor, and superconductivity [46,47].

Adiabatic and vertical ionization potentials (IPs) were examined for eight armchair BNNTs with diameters ranging from 4.32 to 14.23 Å. The DFT results are presented in Fig. 7. and Table 2. As mentioned above, the adiabatic IP is described as the minimum amount of energy required to remove an electron from a neutral molecule. In Fig. 7, the first observation to be made is that both adiabatic and vertical IPs have started from either energy. In addition, both adiabatic and vertical IPs, as well as the energy gap, present a regular decrease in increasing the BNNT diameter. The curves of adiabatic and vertical IPs do not display straight-line behavior. For small diameter BNNTs, the mentioned values are larger than the larger ones. As it is clear in Fig. 7, the 3 × 3×3 BNNT possesses the maximum value, then it decreases slightly. Its reduction trend is the same for other large diameter BNNTs, as well. Furthermore, vertical IP values of 3 × 3×3 and 4 × 4×3 BNNTs are higher than other BNNTs and thus a removal electron is relatively difficult for these BNNTs.

In the literature, there are no available theoretical or experimental studies on adiabatic and vertical IPs of BNNTs for comparison, while results are consistent with previous theoretical calculations and experimental studies for CNTs [48].

Fig. 8 depicts the chemical hardness (η) and maximum amount of electronic charge index (ΔN_{tot}) of BNNTs. The calculated η and ΔN_{tot} are presented in Table 2. The η is not resistant to mechanical deformation, that is, it is defined as the resistance to alter in the electron numbers in the system, deformation of the electron in molecules, or change in the one-electron density function [49]. According to Ref. [50], the η is just half the energy gap as defined in computational part. Therefore, it can be expressed that large energy gap corresponds a hard system and small one is soft. As it is obvious from the calculation results which are summarized in Fig. 8, the obtained positive values imply that free electron transfer to the BNNT is desirable for all BNNTs. The value of η for 3 × 3×3 BNNT is higher than those of other BNNTs and thus higher resistance to charge transfer. Herein, the charge transfer values (in units of e) between BNNT and CO from 3 × 3×3 to 10 × 10 × 3 type BNNTs are found to be -0.37, 0.32, 0.26, 0.19, 0.24, 0.14, 0.23 and 0.23, respectively. It is obvious that the η remarkably decreases for larger BNNTs and a similar decreasing trend is seen for 5 × 5×3 and 6 × 6×3 BNNTs, while the η is identical for 7 × 7×3 and larger BNNTs. It should

Table 2
The electronic properties and reactivity parameters (in eV) of BNNTs.

Models	HOMO	LUMO	E_g	AIP	VIP	η	ω	ΔN_{tot}
3 × 3×3	−6.63	−0.31	6.32	7.86	7.94	3.16	0.00	0.05
4 × 4×3	−6.59	−0.37	6.22	7.71	7.77	3.11	0.01	0.06
5 × 5×3	−6.60	−0.39	6.22	7.62	7.66	3.11	0.01	0.06
6 × 6×3	−6.61	−0.39	6.23	7.55	7.58	3.11	0.01	0.06
7 × 7×3	−6.62	−0.39	6.23	7.49	7.51	3.12	0.01	0.06
8 × 8×3	−6.62	−0.38	6.24	7.43	7.45	3.12	0.01	0.06
9 × 9×3	−6.63	−0.38	6.25	7.38	7.40	3.12	0.01	0.06
10 × 10 × 3	−6.60	−0.40	6.20	7.34	7.36	3.10	0.01	0.06

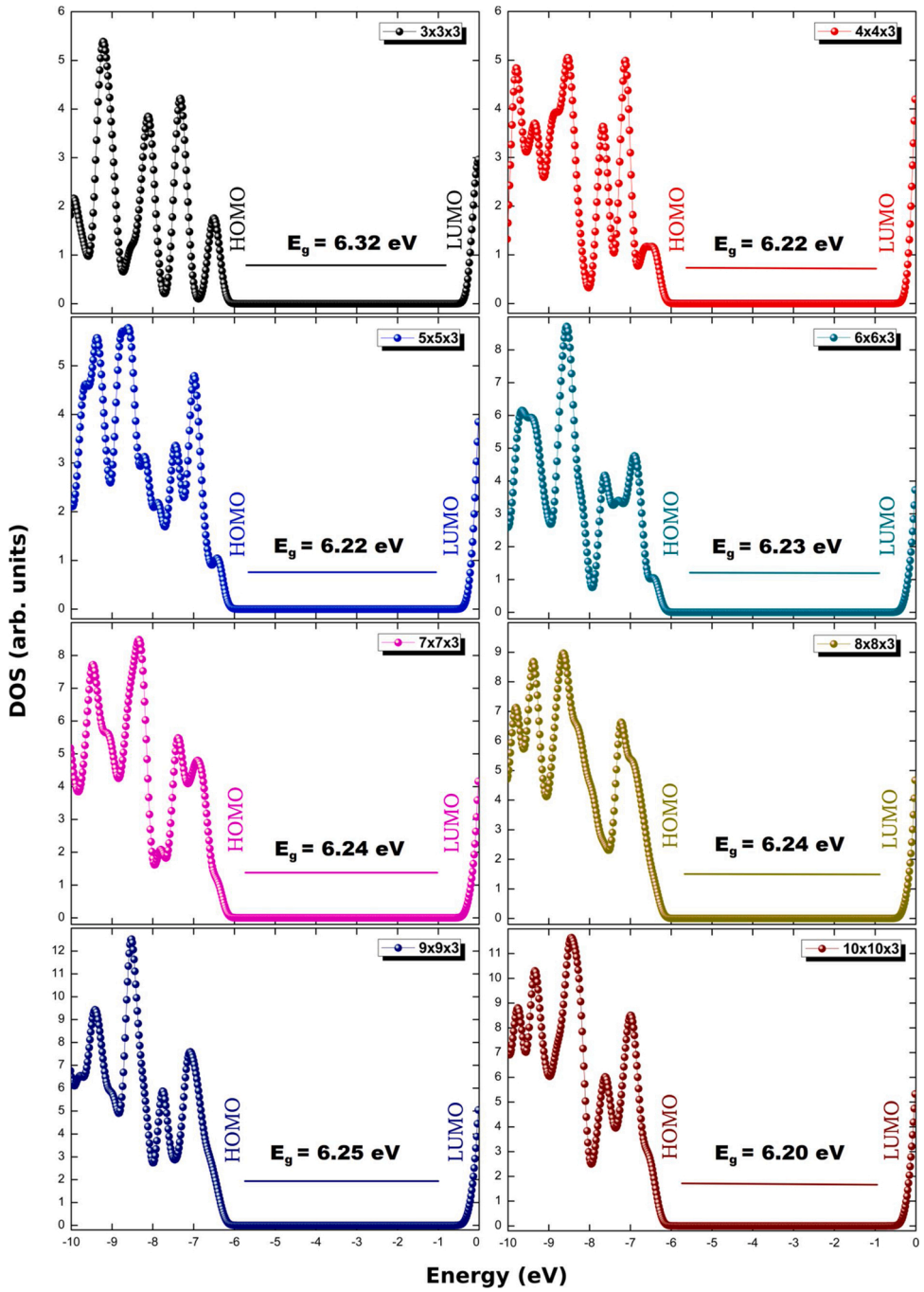

Fig. 6. The density of states (DOS) of BNNTs.

be mentioned that higher η values eventuate in the harder structure, thus the smaller electron affinity as well as larger ionization potential and large energy gap. The maximum amount of electronic charge index (ΔN_{tot}) is a measure of the electron accepting ability of the system. From the results of Fig. 8, it can be perceived that the diameter rise of the BNNTs is associated with an increase in the ΔN_{tot}. A similar trend has been achieved for carbon and aluminum nitride nanotubes with different diameters in the literature [38,39].

Absorbance spectra of BNNTs with different diameters as a function of wavelength were demonstrated in Fig. 9. The BNNTs exhibit strong absorption peaks ~7.08 eV corresponds to the far-ultraviolet (UV) region. The other band at ~6.52 eV is due to the intrinsic dark exciton absorption. The predicted optical band gap (~7.08 eV) is larger than an experimental value (~5.9 eV) [51]. The one reason of this difference probably results from quantum confinement effects [52,53] because the diameter of experimental BNNTs is in the range of 10–100 nm, but we have carried out only up to ~14 nm. The other reason is that the measurement was performed in a solvent environment which gives rise to a shift in the wavelength when compared to the gas environment [54].

To understand the nature of bonding behavior between the BNNTs and CO, we have performed a topological analysis of the electron localization function (ELF) using the Multiwfn program [55]. Fig. 10 shows the ELF for adsorption behavior of 3 × 3×3, 5 × 5×3, 8 × 8×3 and 10 × 10 × 3 BNNTs upon CO. ELF value of the bond between CO and 3 × 3×3 BNNT is slightly more than these of 5 × 5×3, 8 × 8×3 and 10 × 10 × 3 BNNTs. However, the ELF values demonstrate notable changes by increasing the radius of BNNTs when compared with the 3 × 3×3 BNNT. The blue regions exist between CO and BNNT, which

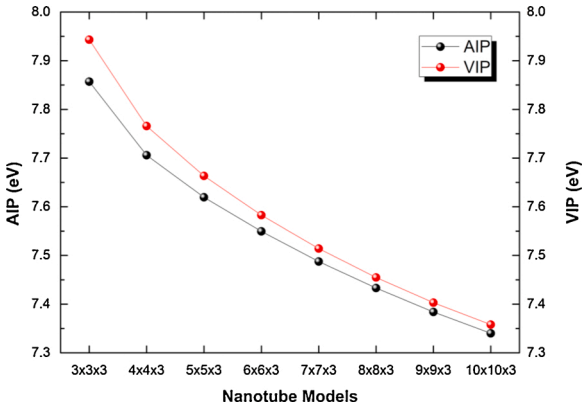

Fig. 7. Adiabatic ionization potential (AIP) and vertical ionization potential (VIP) of BNNTs.

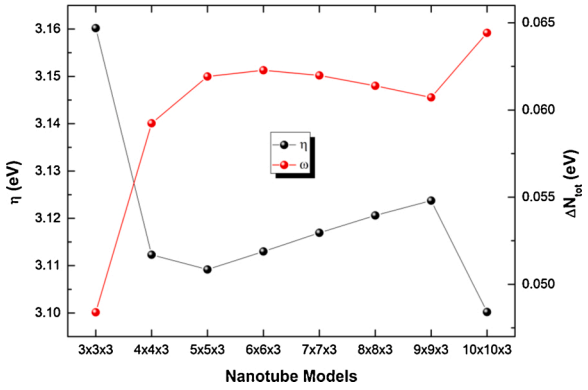

Fig. 8. Chemical hardness (η) and maximum amount of electronic charge index (ΔN_{tot}) of BNNTs.

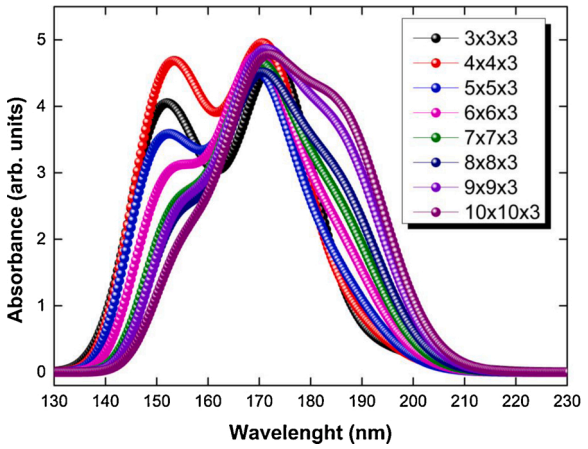

Fig. 9. The UV–vis absorption spectra of BNNTs.

means that there is no chemical interaction between BNNT and CO. This indicates that CO is physically adsorbed on BNNTs (except 3 × 3×3 BNNT) by the weak van der Waals (vdW) interaction, which provides good desorption efficiency for gas molecule and re-use of a biosensor.

4. Conclusion

In summary, the diameter-dependent electronic structure of BNNTs and CO-BNNTs interactions with different diameters have been investigated based on DFT calculations. Firstly, the HOMO, LUMO, HOMO-LUMO energy gap, binding energy, DOS, adiabatic and vertical ionization potentials, chemical hardness, and electrophilicity index are studied to get a better insight into the role of the diameter of BNNTs. Our results reveal that an increment in the diameter of BNNTs causes a rise in the binding energy from 6.44 eV to 6.62 eV. The gap energy gap of BNNT with the biggest diameter is calculated as 6.20 eV wide, i.e., about 0.12 eV smaller than the smallest one. Secondly, the adsorption energy of CO upon BNNTs was examined. A considerable increase in the diameter of BNNTs could enhance the sensing capability of BNNT over CO. Finally, we have performed the TD-DFT method to study the

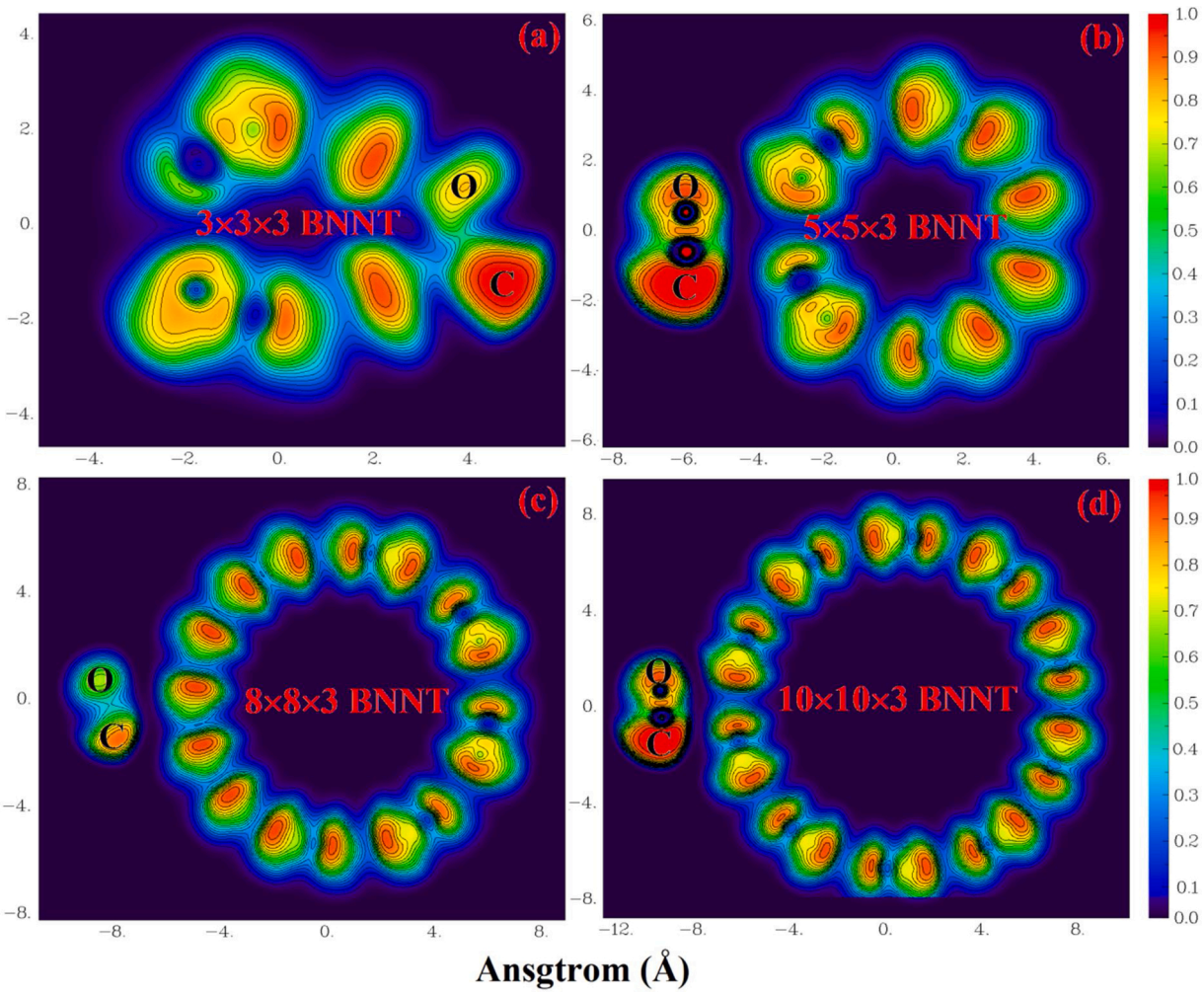

Fig. 10. Electron localization function (ELF) for optimized structures of CO molecule upon the surface of (a) 3 × 3×3 (b) 5 × 5×3 (c) 8 × 8×3 and (d) 10 × 10 × 3 BNNTs.

absorption spectra. The BNNTs exhibit strong absorption peaks of ~7.08 eV which can be hopeful for the UV light-emitting devices. In addition, ELF analyses indicate that BNNTs can be a potential tool for detecting CO. We expect that the obtained results in this study provide useful information diameter-dependent and the sensing capability of BNNTs with different diameters for gas sensor devices.

CRediT authorship contribution statement

İskender Muz: Investigation, Visualization, Methodology, Conceptualization, Writing - original draft, Writing - review & editing, Data curation, Software. **Sholeh Alaei:** Investigation, Writing - review & editing. **Mustafa Kurban:** Supervision, Investigation, Writing - original draft, Writing - review & editing, Data curation, Validation.

Declaration of Competing Interest

The authors report no declarations of interest.

Acknowledgments

The numerical calculations reported were partially performed at TUBITAK ULAKBIM, High Performance and Grid Computing Centre (TRUBA resources), Turkey.

References

[1] Angel Rubio, Jennifer L. Corkill, Marvin L. Cohen, Theory of graphitic boron nitride nanotubes, Phys. Rev. B 49 (7) (1994) 5081.
[2] Nasreen G. Chopra, et al., Boron nitride nanotubes, Science 269 (5226) (1995) 966–967.
[3] X. Blase, et al., Stability and band gap constancy of boron nitride nanotubes, EPL (Europhysics Letters) 28 (5) (1994) 335.
[4] Ernesto Chigo Anota, Gregorio H. Cocoletzi, First-principles simulations of the chemical functionalization of (5, 5) boron nitride nanotubes, J. Mol. Model. 19 (6) (2013) 2335–2341.
[5] A.Rodríguez Juárez, et al., Stability and electronic properties of armchair boron nitride/carbon nanotubes, Fuller. Nanotub. Carbon Nanostructures 25 (12) (2017) 716–725.
[6] Ernesto Chigo Anota, et al., Physicochemical properties of armchair non-stoichiometric boron nitride nanotubes: a density functional theory analysis, Superlattices Microstruct. 89 (2016) 319–328.
[7] D. Golberg, et al., Nanotubes in boron nitride laser heated at high pressure, Appl. Phys. Lett. 69 (14) (1996) 2045–2047.
[8] J.S. Lauret, et al., Optical transitions in single-wall boron nitride nanotubes, Phys. Rev. Lett. 94 (3) (2005) 037405.
[9] Zhuhua Zhang, Wanlin Guo, Yitao Dai, Stability and Electronic Properties of Small BN Nanotubes, arXiv preprint arXiv:0807.0884, 2008.
[10] Homin Shin, et al., Covalent functionalization of boron nitride nanotubes via reduction chemistry, ACS Nano 9.12 (2015) 12573–12582.
[11] Jing-Xiang Zhao, Bai-Qing Dai, DFT studies of electro-conductivity of carbon-doped boron nitride nanotube, Mater. Chem. Phys. 88 (2-3) (2004) 244–249.
[12] Yuri F. Zhukovskii, et al., Ab initio simulations on the atomic and electronic structure of single-walled BN nanotubes and nanoarches, J. Phys. Chem. Solids 70 (5) (2009) 796–803.
[13] Mauricio Terrones, et al., Pure and doped boron nitride nanotubes, Mater. Today 10 (5) (2007) 30–38.

[14] Sheetal Sharma, et al., Structural and electronic properties of sulphur-doped boron nitride nanotubes, Solid State Commun. 152 (9) (2012) 802–805.
[15] Mahmoud Mirzaei, Azita Nouri, The Al-doped BN nanotubes: a DFT study, J. Mol. Struct. Theochem 942 (1-3) (2010) 83–87.
[16] Ruoxi Wang, Rongxiu Zhu, Dongju Zhang, Adsorption of formaldehyde molecule on the pristine and silicon-doped boron nitride nanotubes, Chem. Phys. Lett. 467 (1-3) (2008) 131–135.
[17] Aziz Habibi-Yangjeh, Hadi Basharnavaz, Adsorption of HCN molecules on Ni, Pd and Pt-doped (7, 0) boron nitride nanotube: a DFT study, Mol. Phys. 116 (10) (2018) 1320–1327.
[18] Baoli Zeng, et al., First-principles study on the adsorption of hydrogen cyanide on the metal-doped (8, 0) boron nitride nanotubes, Chem. Phys. Lett. 730 (2019) 513–520.
[19] You Xie, Yi-Ping Huo, Jian-Min Zhang, First-principles study of CO and NO adsorption on transition metals doped (8, 0) boron nitride nanotube, Appl. Surf. Sci. 258 (17) (2012) 6391–6397.
[20] Mahboobeh Amiri Fadradi, Tayebeh Movlarooy, Ab initio study of adsorption of CO on BNNTs: for gas nanosensor applications, Mater. Chem. Phys. 215 (2018) 360–367.
[21] Ruoxi Wang, Dongju Zhang, Chengbu Liu, The germanium-doped boron nitride nanotube serving as a potential resource for the detection of carbon monoxide and nitric oxide, Comput. Mater. Sci. 82 (2014) 361–366.
[22] Preeti Singla, Sonal Singhal, Neetu Goel, Theoretical study on adsorption and dissociation of NO2 molecules on BNNT surface, Appl. Surf. Sci. 283 (2013) 881–887.
[23] Yu-qing Zhang, et al., Boosting sensitivity of boron nitride nanotube (BNNT) to nitrogen dioxide by Fe encapsulation, J. Mol. Graph. Model. 51 (2014) 1–6.
[24] M. Rezaei-Sameti, V. Padervand, A computational study of hydrogen cyanide interaction with the pristine and B, Ga, BGa-doped of (8, 0) zigzag AlPNTs, J. Incl. Phenom. Macrocycl. Chem. 86 (3-4) (2016) 359–373.
[25] Zhen Zhou, et al., Comparative study of hydrogen adsorption on carbon and BN nanotubes, J. Phys. Chem. B 110 (27) (2006) 13363–13369.
[26] Nianduan Lu, et al., Investigation of adsorbed small-molecule on boron nitride nanotube (BNNT) based on first-principles calculations. 2018 International Conference on Simulation of Semiconductor Processes and Devices (SISPAD, IEEE, 2018.
[27] Maziar Noei, Ali Ahmadi Peyghan, A DFT study on the sensing behavior of a BC 2 N nanotube toward formaldehyde, J. Mol. Model. 19 (9) (2013) 3843–3850.
[28] Kriengkri Timsorn, Chatchawal Wongchoosuk, Adsorption of NO2, HCN, HCHO and CO on pristine and amine functionalized boron nitride nanotubes by self-consistent charge density functional tight-binding method, Mater. Res. Express 7 (5) (2020) 055005.
[29] Yunguo Li, Rajeev Ahuja, J. Andreas Larsson, Communication: Origin of the Difference Between Carbon Nanotube Armchair and Zigzag Ends, 2014, p. 091102.
[30] Axel D. Becke, A new mixing of Hartree–Fock and local density-functional theories, J. Chem. Phys. 98 (2) (1993) 1372–1377.
[31] M.J. Frisch, G.W. Trucks, H.B. Schlegel, G.E. Scuseria, M.A. Robb, J.R. Cheeseman, G. Scalmani, V. Barone, B. Mennucci, G.A. Petersson, H. Nakatsuji, M. Caricato, X. Li, H.P. Hratchian, A.F. Izmaylov, J. Bloino, G. Zheng, J.L. Sonnenberg, M. Hada, M. Ehara, K. Toyota, R. Fukuda, J. Hasegawa, M. Ishida, T. Nakajima, Y. Honda, O. Kitao, H. Nakai, T. Vreven, J.A. Montgomery, J.E. Peralta, F. Ogliaro, M. Bearpark, J.J. Heyd, E. Brothers, K.N. Kudin, V.N. Staroverov, R. Kobayashi, J. Normand, K. Raghavachari, A. Rendell, J.C. Burant, S.S. Iyengar, J. Tomasi, M. Cossi, N. Rega, J.M. Millam, M. Klene, J.E. Knox, J.B. Cross, V. Bakken, C. Adamo, J. Jaramillo, R. Gomperts, R.E. Stratmann, O. Yazyev, A.J. Austin, R. Cammi, C. Pomelli, J.W. Ochterski, R.L. Martin, K. Morokuma, V.G. Zakrzewski, G.A. Voth, P. Salvador, J.J. Dannenberg, S. Dapprich, A.D. Daniels, J.B.F. oresman Farkas, J.V. Ortiz, J. Cioslowski, D.J. Fox, Gaussian 09., Revision E.01.01, Gaussian Inc., Wallingford C.T, 2009.
[32] Stefan Grimme, Stephan Ehrlich, Lars Goerigk, Effect of the damping function in dispersion corrected density functional theory, J. Comput. Chem. 32.7 (2011) 1456–1465.
[33] Noel M. O'boyle, Adam L. Tenderholt, Karol M. Langner, Cclib: a library for package-independent computational chemistry algorithms, J. Comput. Chem. 29.5 (2008) 839–845.
[34] Tjalling Koopmans, Über die Zuordnung von Wellenfunktionen und Eigenwerten zu den einzelnen Elektronen eines Atoms, Physica 1 (1-6) (1934) 104–113.
[35] Takeshi Yanai, David P. Tew, Nicholas C. Handy, A new hybrid exchange–correlation functional using the Coulomb-attenuating method (CAM-B3LYP), Chem. Phys. Lett. 393 (1-3) (2004) 51–57.
[36] Mustafa Kurban, Bayram Gündüz, Fahrettin Göktaş, Experimental and theoretical studies of the structural, electronic and optical properties of BCzVB organic material, Optik 182 (2019) 611–617.
[37] Ofir E." Alon, Symmetry properties of single-walled boron nitride nanotubes, Phys. Rev. B 64 (15) (2001), 153408.
[38] Iskender Muz, Mustafa Kurban, A comprehensive study on electronic structure and optical properties of carbon nanotubes with doped B, Al, Ga, Si, Ge, N, P and As and different diameters, J. Alloys Compd. 802 (2019) 25–35.
[39] İskender Muz, Hasan Kurban, Mustafa Kurban, A DFT Study on Stability and Electronic Structure of AlN Nanotubes, Mater. Today Commun. 26 (2021) 102118.
[40] Ying Chen, et al., A solid-state process for formation of boron nitride nanotubes, Appl. Phys. Lett. 74 (20) (1999) 2960–2962.
[41] G.G. Fuentes, et al., Electronic structure of multiwall boron nitride nanotubes, Phys. Rev. B 67 (3) (2003) 035429.
[42] Mosahhar Bagheri, et al., Electronic and structural properties of Au-doped zigzag boron nitride nanotubes: a DFT study, Solid State Commun. 189 (2014) 1–4.
[43] Chunyi Zhi, et al., Boron nitride nanotubes, Mater. Sci. Eng. R Rep. 70 (3-6) (2010) 92–111.
[44] S. Niyogi, et al., Chemistry of single-walled carbon nanotubes, Acc. Chem. Res. 35 (12) (2002) 1105–1113.
[45] Ernesto Joselevich, Electronic structure and chemical reactivity of carbon nanotubes: a chemist's view, ChemPhysChem 5.5 (2004) 619–624.
[46] Ralph Krupke, et al., Separation of metallic from semiconducting single-walled carbon nanotubes, Science 301 (5631) (2003) 344–347.
[47] Debjit Chattopadhyay, Izabela Galeska, Fotios Papadimitrakopoulos, A route for bulk separation of semiconducting from metallic single-wall carbon nanotubes, J. Am. Chem. Soc. 125.11 (2003) 3370–3375.
[48] F. Buonocore, et al., Ab initio calculations of electron affinity and ionization potential of carbon nanotubes, Nanotechnology 19 (2) (2007), 025711.
[49] Ralph G. Pearson, The principle of maximum hardness, Acc. Chem. Res. 26 (5) (1993) 250–255.
[50] Ralph G. Pearson, Absolute electronegativity and hardness correlated with molecular orbital theory, Proc. Natl. Acad. Sci. 83 (22) (1986) 8440–8441.
[51] Chee Huei Lee, et al., Effective growth of boron nitride nanotubes by thermal chemical vapor deposition, Nanotechnology 19 (45) (2008) 455605.
[52] Hasan Kurban, Mustafa Kurban, Mehmet Dalkılıç, Density-functional tight binding approach for the structural analysis and electronic structure of copper hydride metallic nanoparticles, Mater. Today Commun. 21 (2019) 100648.
[53] Mustafa Kurban, Size-and composition-dependent structure of ternary Cd-Te-Se nanoparticles, Turk. J. Phys. 18 (2018) 19.
[54] Mustafa Kurban, Bayram Gündüz, Electronic structure, optical and structural properties of organic 5, 5′-Dibromo-2, 2′-bithiophene, Optik 165 (2018) 370–379.
[55] Tian Lu, Feiwu Chen, Multiwfn: a multifunctional wavefunction analyzer, J. Comput. Chem. 33.5 (2012) 580–592.